Solving the Infrared Reflections Contribution by Inversion of Synthetic Diagnostics: first results on WEST

Charly Talatizi[a*], Marie-Hélène Aumeunier[a], Fabrice Rigollet[b], Mickael Le Bohec[b], Christophe Le Niliot[b], Albrecht Herrmann[c]

[a]*CEA Cadarache/Institut de Recherche sur la Fusion par confinement Magnétique, 13108 Saint-Paul-lez-Durance cedex, France*
[b]*Aix Marseille Univ., CNRS, IUSTI UMR 7343, Marseille, France*
[c]*Max-Planck-Institut für Plasmaphysik, EURATOM Association, Boltzmannstr. 2, D-85748 Garching, Germany*
[*]*Corresponding author: marie-helene.aumeunier@cea.fr*

Infrared (IR) diagnostics are used to measure plasma-facing components (PFC) surface temperature in fusion devices. However, the interpretation of such images is complex in all-reflective environments because of unknown emissivity and multiple reflections issues. In order to assess these challenges an iterative inversion method based on a fast photonic model, the radiosity method, has been developed. This method is applied to two different direct models based on different geometries, Sec-Tore and RADIOS, in order to estimate temperatures from experimental-like data simulated with a Monte Carlo ray-tracing code with diffuse reflective surfaces or specularly reflective surfaces. RADIOS allows retrieving temperature on colder targets (lower than 200°C) with errors of 33% and the peak temperatures with errors of 6%.

Keywords: infrared thermography, emissivity, reflections, Ray Tracing Monte Carlo, Radiosity method, inverse problem

1. Introduction

In fusion devices, infrared (IR) cameras are key diagnostics to monitor Plasma-Facing Components (PFC) submitted to high heat flux (10MW/m^2 in steady-state, up to 20MW/m^2). Measuring accurately PFC surface temperature is also mandatory to ensure machine protection and optimize plasma operation. For example, the WEST device is equipped with 12 IR cameras looking at the First Wall (FW), the heating antennas and the divertor, the most critical component receiving heat flux up to 20 MW/m² [1].

Nevertheless, the use of all-metallic materials (mainly stainless steel, tungsten and beryllium) with low and variable emissivity ($\varepsilon \sim 0.1\text{-}0.3$ in the IR bandwidth considered $[3\mu m, 5\mu m]$) makes the surface temperature measurement difficult [1]. Indeed, the radiance collected by the IR camera includes both the thermal radiation emitted by the target and a parasitic radiation coming from the surroundings of the target. Furthermore, target emissivity changes with the surface temperature. This causes major errors on the surface temperature measurement that we need to address in order to achieve high power and safe plasma operation.

IR synthetic diagnostic has been used to quantify accurately, for each camera, the impact on the surface temperature measurement of inaccurate emissivity, the reflections and camera resolution [2]-[4]. The use of this synthetic diagnostic has proven that this can lead to major errors on surface temperature measurement up to 100% for colder targets (temperature lower than 150°C) and 50% for hot targets (maximum temperature around 1300°C).

This paper presents the results of an inverse method aiming to retrieve the true surface temperature of the PFC by solving low emissivity and additional parasitic flux coming from the reflections. This method relies on the comparison and the least squares minimization between the experimental IR image and a synthetic IR image (obtained through a direct model or forward model). Two reduced photonic models have been developed, tested and compared on WEST tokamak-like numerical prototype.

2. Generating IR images

In a first step, the inverse method proposed in this paper has been developed and tested from IR simulated images generated with a synthetic diagnostic. This synthetic diagnostic is based on a Monte Carlo ray-tracing (MCRT) code of ANSYS-SPEOS company [5] able to propagate rays in 3D geometry taking into account complex thermo-radiative properties of materials and inhomogeneous 3D temperature fields as inputs. Geometrical camera parameters (focal length, detector size) are used to reproduce the 2D IR image and the collected radiance by each pixel.

The MCRT code is currently the most sophisticated and reliable code to deal with complex geometrical and physics models and so generate realistic infrared images. Nevertheless, it is not so far adapted to deal with the forward relation between data and model parameters for the nonlinear inverse problem we want to address here; especially due to the required computing time (10 hour with 4 cores to generate a synthetic image with 2-3% precision). This leads to develop reduced direct models able to compute quickly the IR images under some assumptions and approximations described in section 3. In this paper the MCRT is used for generating experimental-like synthetic data as replacement of the experimental data in order to test the developed inverse method and its range of validity.

Figure 1 describes the thermal scene used as benchmark to test the proposed method aiming to retrieve the surface temperature by filtering reflections. In this first step, a simplified geometry of the vessel is considered without including specific components such as the heating antennas, the bumpers and so on. In the same way, a uniform temperature (fixed at 90 °*C*) is considered for the first wall, the upper divertor and the baffle. The emissivity value is also assumed uniform and fixed for each component. Even though these considerations do not accurately reflect the reality, this first step is mandatory to demonstrate the method validity and performance. A temperature profile is applied on the lower divertor that roughly reproduces the heat loads in a tokamak with two strike points and a toroidal modulation of a 20° period to reproduce the ripple effect. The considered materials are Tungsten for the lower divertor, the baffle and the upper divertor with an emissivity of 0.1 and Stainless Steel for the first wall with an emissivity of 0.3 fitting roughly with the literature [6]. The camera model reproduces the view of WEST standard divertor view [1] with a spectral IR range of $\Delta\lambda$=4.3 µm – 4.4 µm. The precision of simulated IR map will depend on the number of rays launched in the MCRT code. The simulated experimental images are characterized by a statistic noise around 2% of the collected radiance for colder targets.

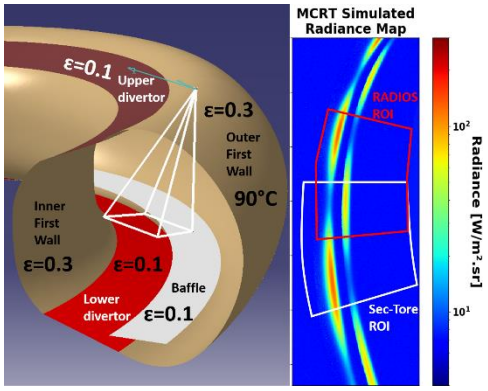

Figure 1 – Geometry used as input of the MCRT simulation (left) and the resulting simulated IR image (right)

3. Inverse method

3.1 Approach description

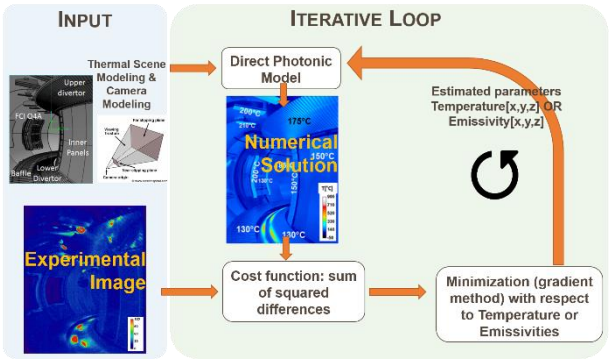

Figure 2 – Illustration of the iterative inversion method developed to retrieve temperature or emissivity

The inverse method relies on iterative loop as described in Figure 2 which consists in retrieving the model's parameters (here temperature) by minimizing the difference between experimental and simulated data. The simulated data comes from a direct photonic model. In this paper, two direct models are tested and compared: a simplified model so-called Sec-tore (section 3.2.2) and a reduced model so-called RADIOS (section 3.3.3). In [7], the inversion method is tested in an inverse crime situation meaning that the synthetic data used to replace the experimental data come from the same forward model used for inversion, with an additive Gaussian white noise. In this paper, the experimental-like data are simulated with an independent and more sophisticated code described in section 2. We are interested in retrieving the surface temperature by solving the reflections but assuming that emissivity is known. Solving the emissivity is also mandatory in a fully reflective environment and is possible with such a method and a first feasibility study is proven in [4]. This assumes known and quite uniform temperatures on the components which can be achieved during specific operations (such as baking and machine conditioning).

3.2 Forward Model

A forward model includes the modeling of tokamak geometry, the thermal scene (3d temperature field), the optical and thermal-radiative properties of materials and the camera. The 3D geometry and the camera model are fixed whereas the 3D distribution of temperature and the optical properties of materials can change. The two developed forward models are based on the same radiosity method (section 3.2.1) to compute the collected flux by camera pixel.

3.2.1 Radiosity Method

The radiosity method is a common method for computing the inter-reflections of light assuming all diffuse reflecting surfaces or Lambertian reflection, meaning that the part of reflected flux is the same in all the directions of observation [8]-[10]. Considering a scene composed of N individual surfaces (patches), the method consists in computing the radiosity $\boldsymbol{J}$ vector *[N]* that contains the total radiation leaving each patch of the scene in all directions per unit area. This energy includes both the emitted energy and the reflected one coming from all the other patches in the enclosure as described in equation *(1)*.

$$\boldsymbol{J} = (\boldsymbol{I} - \boldsymbol{R}(\boldsymbol{\varepsilon})\boldsymbol{F})^{-1}\boldsymbol{\varepsilon}\pi\boldsymbol{L}^{\boldsymbol{0}}(\boldsymbol{T}) \qquad (1)$$

With, $\boldsymbol{I}$ is the identity matrix *[N×N]*, $\boldsymbol{R(\varepsilon)}$ the diagonal reflectivity matrix *[N×N]* where each reflectivity is given by ρ_j=*1-*ε_j *(j=1 to N)*, $\boldsymbol{F} = (\boldsymbol{F_{Aj\to Ak}})$ the view factors matrix *[N×N]* and $\boldsymbol{\pi\varepsilon L^0(T)}$ the emissive power vector *[N]* which is then called the "source term". $\boldsymbol{L^0(T)}$ is the black-body radiance at temperature T given by Planck function integrated in the spectral range of the IR camera. The view factor in the above equation is defined as the fraction (between 0 and 1) of flux leaving the surface A_j and reaching the surface A_k:

$$F_{A_j \to A_k} = \frac{1}{A_j} \int_{A_j} \int_{A_k} \upsilon_{jk} \frac{\cos\theta_j \cos\theta_k}{\pi r_{jk}^2} dA_k dA_j \qquad (2)$$

With υ_{jk} is the obstruction factor between patches j and k, θ_j the angle between the normal of the surface j and the closest distance between the surfaces j and k and θ_k the angle same angle for surface k, A_j is the area of the surface j[8]. For a given geometry, the view factors matrix is computed only once (12 hours with parallel computing). When all the radiosities J_j of the N patches are computed, the 3D to 2D projection is achieved with an OpenGL routine to provide the observable quantity, that is the 2D IR image (made of 640 x 256 pixels) for the given view of the simulated IR camera.

3.2.2 Sec-Tore

Sec-Tore is a simplified model based on a 20° toroidal sector of a numerical prototype of the WEST tokamak closed by two black-body surfaces at the environment temperature. This geometry has been designed in order to prevent any obstruction between two patches of the 3D scene to compute simple view factors (through an integral contour [11]). Sec-Tore is made of N=11.787 patches that lead to a computation of over 69 million view factors. Figure 3 shows the geometry of Sec-Tore and the corresponding modeled image (67.122 pixels) used in the inversion method.

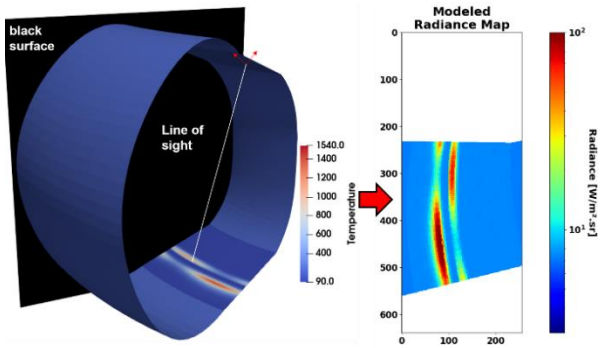

Figure 3 – Illustration of the 3D model of Sec-Tore with a thermal field applied to the mesh (right) and the resulting modeled image after the OpenGL projection (right)

The emissivities of the environment and the lower divertor are assumed known (see Figure 1) as well as the temperature of the environment and the black body surfaces. The 8.796 patches of the lower divertor are regrouped in 1.560 bigger patches. The parameters to be estimated are the 1.560 temperatures of the lower divertor.

3.2.3 RADIOS

RADIOS is a reduced model based on a hierarchical adaptive method [12] allowing to compute only the most important view factors of the scene at the last level of resolution. This criterion of importance is related to the Region of Interest (RoI) of the 3D scene on which are located the parameters to be estimated. The idea is that some initially coarse patches in the whole tokamak are refined (and the corresponding shape factor are computed) only if their contribution to the radiosity of the ROI patches is important (at a given precision level). Such a method allows considering the whole torus (contrary to the Sec-Tore considering only 20° of the tokamak) as well as the obstructions between patches enabling to add more components to the model such as the baffle. Typically, the geometry used in the MCRT code is made of meshes constituted of 2 million elementary surfaces. Without the classical method used in Sec-Tore, 2.10^{12} view factors should be computed, whereas 7.8 million view factors are computed with the hierarchical adaptive method.
Figure 4 shows the mapping of a temperature field on the last level of resolution of the meshes with the ROI identified. The RoI is composed of 1.391 patches, which corresponds to the number of parameters to be estimated in the 3D scene.

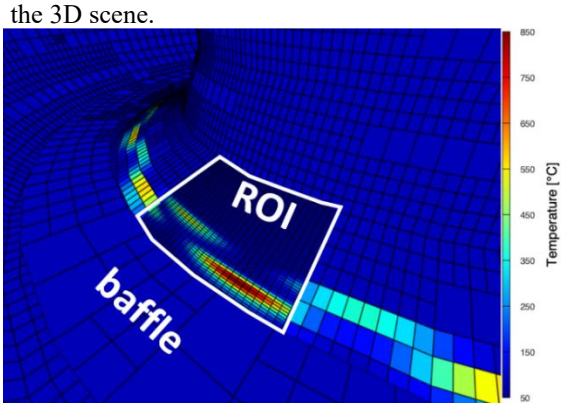

Figure 4 – Illustration of the last level of resolution for a numerical prototype of WEST with the corresponding mapping of temperature

The reduced method RADIOS uses also Gebhart factors as an additional criterion of refinement of the meshes as presented in [13]. As Figure 5 shows, Gebhart factors are a "generalized" version of the view factors taking into account the radiative properties of the patches [14]-[15]. The Gebhart factors between S_j and S_k, also called absorption factors, represent the fraction of the energy initially emitted by S_j that is absorbed finally by S_k, taking into account all the possible reflecting paths in the scene.

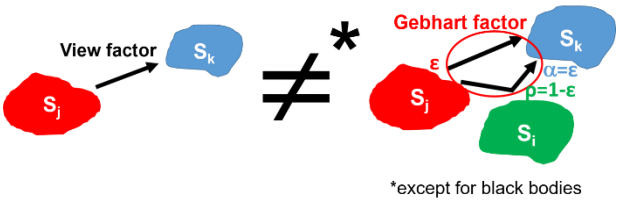

Figure 5 – Usual view factors compared to Gebhart factors taking into account all radiative paths (direct and indirect)

To complete the direct model package the same projection based on OpenGL used for Sec-Tore is applied to RADIOS to produce the final synthetic IR image of the scene.

3.3 Parameters Estimation Problem

The parameters estimation is based on Ordinary Least Squares (OLS) method [17]. The minimization will occur on a RoI of IR images of m pixels. This RoI can be a

profile, an area of image, a list of some particular pixels, etc.

The OLS minimization uses a Gauss-Newton algorithm to update the parameters at each iteration. That is based on the inversion of the $\boldsymbol{S}^T\boldsymbol{S}$ information matrix *[p×p] with p* the numbers of parameters to be estimated:

$$\hat{\boldsymbol{x}}_{OLS}^{(k+1)} = \hat{\boldsymbol{x}}_{OLS}^{(k)} + \left(\boldsymbol{S}^T\boldsymbol{S}\right)^{-1}\boldsymbol{S}^T\left(\boldsymbol{y}_{mes} - \boldsymbol{y}_{\boldsymbol{mo}}\left(\hat{\boldsymbol{x}}_{OLS}^{(k)}\right)\right) \qquad (3)$$

where $\hat{\boldsymbol{x}}_{OLS}$ is the vector of the p parameters to be estimated (temperature here), y_{mes} the vector of m data, y_{mo} the vector of the m outputs of the direct model and k the iteration number.

The specificity of this method is that the estimation is performed on the 3D world (i.e. the parameters are the temperatures of the patches of the divertor) and not on the cameras pixels (2D observable). As a result, the number of parameters p (related to the patches) is not necessarily equal to the number of measurements m *(pixels)* as it depends on the resolution of the camera. Furthermore, some patches that share the same optical/emission properties (in reality or by assumption for modeling) can be gathered into macro patches covered by several pixels, hence different pixels bear the same information regarding one parameter of the model.

Each column j of the sensitivity (or Jacobian) matrix $\boldsymbol{S}$ *[m×p]* contains the sensitivity coefficient of the model to the parameter x_j ($j=1$ *to* p) computed along pixels of interest s_i ($i=1$ *to* m) given by equation *(4)* [16]-[17]:

$$S_j(s_i) = \left.\frac{\partial y_{mo}(s_i,\boldsymbol{x})}{\partial x_j}\right|_{x_k \text{ for } k\neq j}, \; j = 1 \text{ to } p, \; i = 1 \text{ to } m \qquad (4)$$

Nevertheless, as proven in [7], the temperature estimation becomes a linear problem by considering the radiance parameters $L^0(T)$ (related to the temperature T via the Planck function) in equation (3). Then, the radiance parameters can be directly computed with equation (5):

$$\hat{\boldsymbol{L}}_{OLS}^0 = \left(\boldsymbol{S}_r{}^T\boldsymbol{S}_r\right)^{-1}\boldsymbol{S}_r{}^T\left(\boldsymbol{y}_{mes} - \boldsymbol{S}_c\boldsymbol{L}^0{}_c\right) \qquad (5)$$

with, $\boldsymbol{L}^0$ the black body radiance of target from which the temperature will be deduced, $\boldsymbol{S}_r$ the sensitivity matrix for the estimated parameters, $(\boldsymbol{S}_r{}^T\boldsymbol{S}_r)^{-1}\boldsymbol{S}_r{}^T$ the inversion operator, $\boldsymbol{S}_c\boldsymbol{L}^0{}_c$ the reduced sensitivities of the forward model with respect to the known parameters (that is $L^0(T_{env})$ where T_{env} is the temperature of all components in the tokamak except the lower divertor). The vector $\boldsymbol{y}_{shift} = \boldsymbol{y}_{mes} - \boldsymbol{S}_c\boldsymbol{L}^0{}_c$ is called the shifted data. As a result, the solution is quickly computed without any iterations since the problem is linear (four seconds with 16 G0 RAM and 3.5 GHz CPU).

The solution takes also into account the standard deviation σ_i of noise measurement. The noise measurement is considered additive with zero mean and a Gaussian distribution. The standard deviation of the noise is assessed as a constant fraction (typically 2% as indicated in section 2 such as the values obtained from the MCRT simulations) of the radiance collected by each pixel. The noise covariance matrix $\boldsymbol{\Psi}$ is given by *(6)(7)*:

$$\boldsymbol{\Psi} = diag\left[\sigma_1^2 \quad \sigma_2^2 \quad \text{L} \quad \sigma_m^2\right] \qquad (6)$$

The solution of the Maximum Likelihood (ML) estimation [16] is given by equation *(7)*:

$$\hat{\boldsymbol{L}}_{ML}^0 = (\boldsymbol{S}_r{}^T\boldsymbol{\Psi}^{-1}\boldsymbol{S}_r)^{-1}\boldsymbol{S}_r{}^T\boldsymbol{\Psi}^{-1}(\boldsymbol{y}_{mes} - \boldsymbol{S}_c\boldsymbol{L}^0{}_c) \qquad (7)$$

The covariance matrix of ML estimator is given by:

$$\boldsymbol{C} = \text{cov}(\hat{\boldsymbol{L}}_{ML}^0) = (\boldsymbol{S}_r^T\boldsymbol{\Psi}^{-1}\boldsymbol{S}_r)^{-1} \qquad (8)$$

The 95% confidence intervals associated to the ith estimated parameters ($j=1$ *to* p) are computed from the diagonal components of this covariance matrix: $\hat{L}_{ML,j}^0 \pm 1.96\cdot(C_{jj})^{1/2}$.

Table 1 summarizes the main figures for the temperature estimation for Sec-Tore and RADIOS models. The temperature estimation is carried out on a sector of 20° (67.122 pixels for Sec-tore, 49.527 pixels for RADIOS). The estimation with Sec-Tore aims to retrieve the temperature of 1.560 "macro-patches" located on the lower divertor whereas the estimation with RADIOS aims to estimate 1.391 parameters of the patches of 3D ROI of the hierarchical method. RADIOS allows identifying less parameters because some parameters on the outer side of the lower divertor are not monitored by the camera due to the baffle obstruction. The temperature of these patches is assumed equal to the last patches monitored next to the baffle's edge.

Table 1. Main figures for the temperature estimation for Sec-Tore and RADIOS models

Model	Torus part	View factors	m Pixels used	p Parameters estimated
Sec-Tore	20°	69M	67.122	1.560
RADIOS	360°	7.8M	49.527	1.391

4. Results

4.1. Diffuse Case

The first temperature estimation is performed considering a diffuse surface. The synthetic data are generated from the MCRT code, considering purely diffuse reflective materials (or Lambertian reflectance for which the apparent temperature is the same for any observer's angle of view). Two simulated images are generated: one without the baffle for the estimation conducted with Sec-Tore and one with a baffle for the estimation with RADIOS. The emissivities of the components are fixed to their value of the literature (0.1 for the lower divertor, the upper divertor and the baffle, 0.3 for the first wall as stated in section 2 and further to [6]). The temperature of the environment (all surfaces but lower divertor) is assumed known and fixed to its value of 90°C.

Figure 6(a) shows the radiance profiles along the divertor simulated with MCRT considering or not baffle emission: the difference is not significant which allows comparing the results of Sec Tore and RADIOS without bias. This figure also shows the good convergence of the modeled radiance with the Sec-Tore model towards the simulated ones with the MCRT code. Figure 6(b) shows the estimated temperature profiles with both Sec-Tore and RADIOS compared to the true surface temperature used as input of the MCRT simulation.

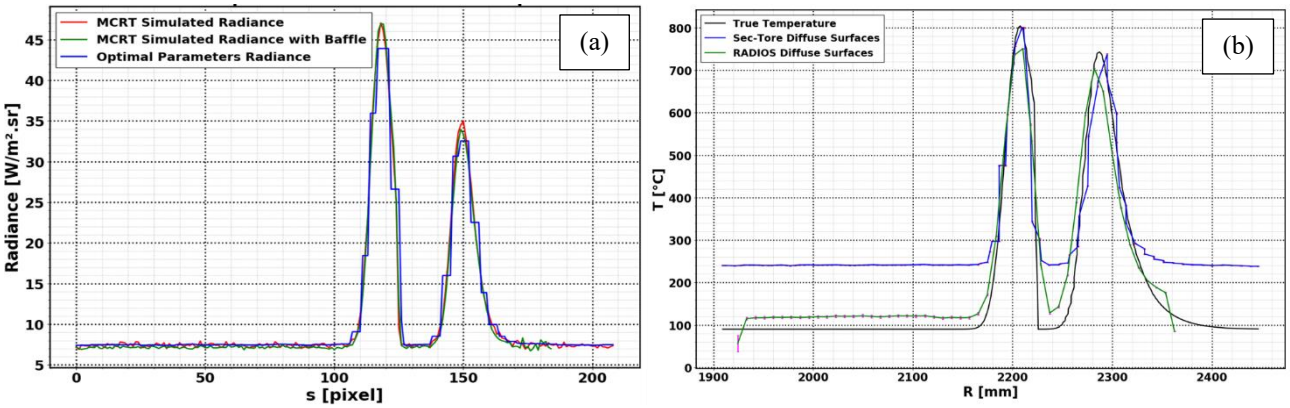

Figure 6 – (a): Synthetic noisy measurements (radiance profiles) built with the MCRT code in the case of diffuse reflective surfaces without baffle (red) and with baffle (green). Comparison with the optimal radiance profile obtained with the temperature estimated by the inverse method Sec Tore (blue). (b): 3D temperature profile estimated with Sec-Tore (blue) with the associated levels of confidence and with RADIOS (green) in the case of synthetic measurements with diffuse reflective surfaces. Profiles correspond to the green lines drawn on the 3D view of Figure 7, the origin being on the inner side.

Sec-Tore enables to estimate the peak temperatures with an error lower than 1% for the maximum temperatures (around 800°C). However, the temperature of the colder part is estimated with an error higher than 166%. This is due to the black-body vertical closing surfaces at T_{env} (see Figure 3) that appear to be a wrong boundary condition to model radiation exchange between the lower divertor and the complete tore (Sec-Tore is limited to a toroidal section of 20°). As expected, RADIOS (modeling the complete 360° tore with hierarchical radiative method) enables to estimate the lower targets temperature with a much lower mean error of 32%. Nevertheless, RADIOS estimation of the peak temperatures is not as good as the Sec-Tore estimation: it is mainly due to the high sensitivity of RADIOS to the noise measurements (synthetized by the MCRT code here). To a slightly lesser extent, these errors can be due to approximations in the forward modeling (approximations of camera viewing and geometry) compared to the real world (here synthetic diagnostic). One should pay peculiar attention when real experimental data will be processed.

Figure 7 shows the mapping of the estimated temperatures for RADIOS and Sec-Tore on the 3D surface compared to the true temperature used as input of the MCRT code.

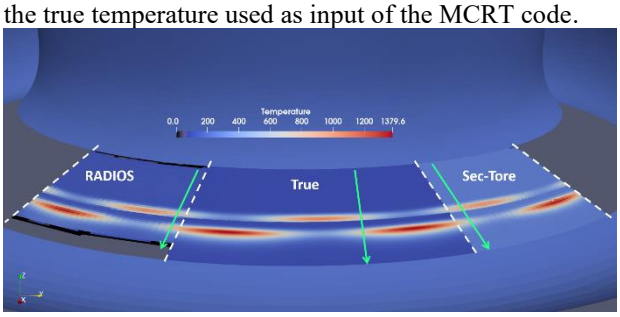

Figure 7 –3D mapping of the estimated temperatures with RADIOS (left) and with Sec-Tore (right) compared to the true temperature used as input of the MCRT code (middle)

The black patches on RADIOS side are parameters that could not be estimated because the model is too sensitive to the noise contained in the simulated data. 110 parameters over 1.391 parameters are not estimated.

4.2. Specular case

The second temperature estimation considers high specular reflectance surface. The synthetic data are generated considering a Bidirectional Reflectance Distribution Function (BRDF) which is a combination of 2% Lambertian reflectance and 98% of specular reflection with a Gaussian distribution of 8° width around the specular direction. Figure 8 compares the simulated images with the MCRT code in case of diffuse and specular surfaces and considering the presence of the baffle.

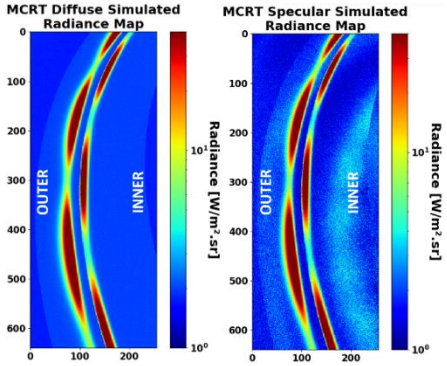

Figure 8 – Synthetics measured radiance maps provided by the MCRT code in the case of fully diffuse reflective surfaces (left) and mainly specular reflective surfaces (right) with logarithmic color bars

Figure 8 shows that the specular reflective materials cause two patterns (halos) of reflections on both side of the strike points: on the inner side of the lower divertor and close to the baffle. These patterns are due to reflections of the environment (vessel wall) at 90°C.

The estimation assumptions are the same as for the diffuse case (environment temperature and emissivities known). Figure 9(a) shows the simulated radiance profile with the MCRT code considering or not the baffle obstruction and

emission. The radiance profiles are quite similar except for the extreme pixels (number 160 and more) impacted by the presence of baffle. There is less signal near the baffle as well as more statistic noise. Concerning the noise, the specular simulations show that the statistic noise represents around 25% of the signal on the colder targets compared to the diffuse relative noise of 2%.
Figure 9 also shows the convergence of the radiance optimal parameters profile (left) and the corresponding results of the estimated 3D temperatures (right).

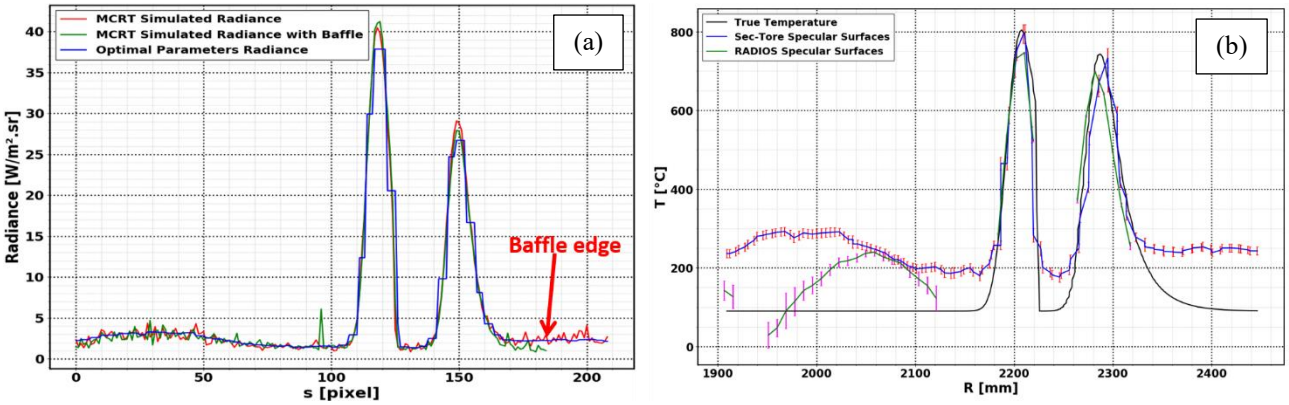

Figure 9 – (a): Synthetic noisy measurements (radiance profiles) built with the MCRT code in the case of specular reflective surfaces without baffle (red) and with baffle (green). Comparison with the optimal radiance profile obtained with the temperature estimated by the inverse method Sec-Tore (blue). (b): 3D temperature profile estimated with Sec-Tore (blue) with the associated levels of confidence and with RADIOS (green) in the case of synthetic measurements with specular reflective surfaces. Profiles correspond to the green lines drawn on the 3D view of Figure 7, the origin being on the inner side.

On one hand, Sec-Tore enables to retrieve all parameters to be estimated. The radiance profiles on Figure 9(a) show the halo of reflection on the inner side in the form of the bump on the left of the profiles (pixels 0 to 70). The convergence of the model regarding the radiances is still good however, the temperature estimation is not so good especially for the halo of reflection. Indeed, the bump on the radiance profile is interpreted by the model as an increased emission of the component in this area and not as a specular pattern of reflection. As a result, the estimated temperature is higher in the matching area (up to 300°C instead of 90°C). The estimated temperature on the colder targets (less prone to reflections) is around 200°C, which represents an error of 120% compared to the previous errors of around 166%. Last, the increase of relative statistic noise on the measurement degrades the confidence levels associated to the temperature estimations (error bars larger than in diffuse case about 2% of the value for Sec-Tore and 4% for RADIOS in diffuse case versus 12% for Sec-Tore and 10-50% for RADIOS in specular case).

On the other hand, RADIOS enables to retrieve only 891 parameters out of the 1.391 estimated parameters (around 60% estimated parameters). This is due to an increase of statistic noise in the simulated experimental-like data when considering specular reflective surfaces. Nevertheless, the estimation of the peak is as good as the estimation considering diffuse reflective surfaces with errors from 1% to 8%. It is worth noting that retrieved parameters out of the peak are the ones located in the area prone to reflections where the halo of reflection is considered by the algorithm as a much hotter zone than it really is.

Figure 10 shows the relative errors on the estimated surface temperature ((estimated-true)/true in %) with Sec-Tore and RADIOS for diffuse reflective surfaces as well as specular reflective surfaces. The true temperature profile used as input of the MCRT code is also plotted to locate the position of the peaks.

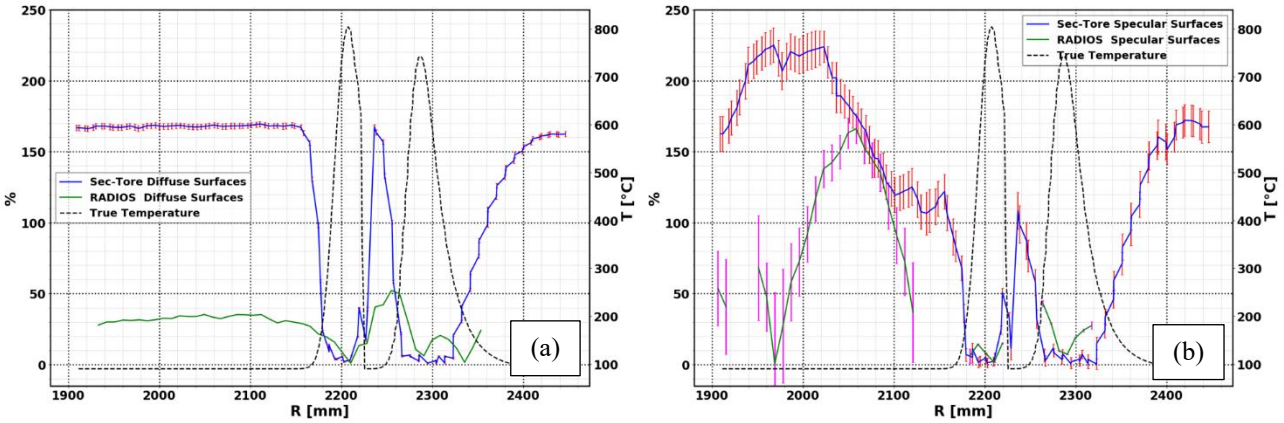

Figure 10 – (a): Relative errors on the estimated temperatures with Sec-Tore for diffuse reflective surfaces (blue) and RADIOS (green) superimposed with the true temperature profile (black). (b): Relative errors on the estimated temperatures with Sec-Tore for specular reflective surfaces (blue) and RADIOS (green) superimposed with the true temperature profile (black). Profiles corresponds to the green lines drawn on the 3D view of Figure 7, the origin being on the inner side.

RADIOS allows estimating less parameters than Sec-Tore because of the presence of the baffle and because some parameters cannot be estimated due to the statistic noise of the simulated data.

Figure 10 shows the mean error of the temperature estimation. As expected the temperature peak at 800°*C*, which is less affected by parasitic reflections, is retrieved with a good accuracy (better than 1% both for diffuse and specular surfaces). The advantage of the RADIOS model (considering the whole torus) is quite proven for colder targets (temperature around 90°*C*) in the diffuse case since it allows reducing the surface temperature error to 33% from 166% with the Sec-Tore model. The specular case is more complicated to analyze. Indeed, the additional parasitic light coming from specular reflection is not uniform along the target due to angular dependence of reflectivity. As a result, a kind of bump is observed along the luminance profile (Figure 10b). As the model used for the inversion assumes Lambertian reflections, the bump is interpreted as an increase of emittance and so the algorithm finds a solution with a higher temperature than expected. This leads to larger temperature errors using both models Sec-Tore and RADIOS up to more than 200%.This illustrates and quantify the limits of the radiosity method considering diffuse reflecting surfaces to retrieve temperatures of specular reflecting surfaces. The next step should be to enhance the direct model taking into account the specular behavior of the reflectance model based on previous studies as described in [19].

Table 2 summarizes the results of the temperature estimation with both Sec-Tore and RADIOS for diffuse reflective surfaces and specularly reflective surfaces. RADIOS gives results of temperature estimation with a mean error of 32% on the colder targets and 1 to 8% error for the peak temperature. As mentioned in section 4.1 this degradation of the peak temperature estimation is due to approximations in the modeling of RADIOS and noise statistic.

Table 2. Comparison of the results estimation with Sec-Tore and RADIOS.

Reflection model	Temperature location	Sec-Tore	RADIOS
Diffuse	Hot Peak	1%	6%
	Cold targets	166%	33%
Specular	Hot Peak	< 1%	/
	Cold targets	106%-223%	/

5. Conclusion

This paper presents the results of an inverse method aiming to retrieve the true surface temperature from IR measurements solving low emissivity and the additional parasitic flux coming from the reflections. In the inverse method presented here, the temperature estimation is carried out with two different forward radiative models, both using radiosity calculations but based on two different geometries: Sec-Tore and RADIOS. On one hand, Sec-Tore only considers a toroidal 20° sector of a tokamak closed by two black-body surfaces with very simple components and no obstructions between elementary patches. On the other hand, RADIOS considers a whole torus and can deal with obstructions between patches and then can include more realistic components such as the baffle into the model. To test the method, the IR measurements are replaced by synthetic experimental-like data simulated with a MCRT code considering diffuse or highly specular reflective surfaces. In the case of diffuse reflective surfaces, Sec-Tore gives good results for the peak temperature estimation with error of 1%. However, due to the boundary condition of black body surfaces closing the 20° sector, the error on colder targets temperature estimation reaches 166%. RADIOS gives better results for the colder targets temperature estimation with a mean of error of 32% but the peak temperature estimation is degraded by approximations in the modeling, with respect to the MCRT code that generated the synthetic data (geometry sometimes simplified to limit the number of total

patches). The temperature estimations with RADIOS is also currently limited by the sensitivity of the inversion process to the noise existing on the synthetic measurements. This leads to the impossibility to estimate some parameters. These issues should be reduced by improving the conditioning of the model by using regularization methods (such as Tikhonov regularization [19]), optimization under constraints or with a priori values of some parameters.

In the case of specular reflective surfaces, the temperature estimation with Sec-Tore and RADIOS still gives good results for the peak temperature, but the temperature estimation of colder targets, prone to reflections, is more chaotic with great errors. This result was expected as the radiosity method assumes diffuse surfaces and cannot interpret specular patterns of reflection. The next challenge will be to take into account specular surfaces in RADIOS.

Nevertheless, the developed inverse method has proved very promising for retrieving the true temperature by filtering reflections. Furthermore, as the temperature estimation problem is linear and relies only on a matrix product based on the pre-computed and stored Jacobian (eq. *(7)*), this inverse method could be compatible with real-time application.

Acknowledgements

This work has been carried out within the framework of the EUROfusion Consortium and has received funding from the EURATOM research and training programme 2019-2020 under grant agreement No 633053. The views and opinions expressed herein do not necessarily reflect those of the European Commission.

References

[1] Courtois X. et al, Design and status of the new WEST IR thermography system, ISFNT 2017.

[2] Aumeunier M.-H. et al, 2017, *Nuclear Materials and Energy* 12, Pages 1265-1269.

[3] Aumeurnier M.-H. et al., 2012, IEEE Transactions on Plasma Science, 40, 3.

[4] Talatizi C. et al., Thermique et sciences de l'information, Tome1, Actes du Congrès annuel de la Société Française de Thermique, SFT 2018 (ISBN : 978-2-905267-95-5).

[5] https://www.ansys.com/products/optical/ansys-speos

[6] Touloukian Y., 1967, *Thermophysical properties of high temperature solid materials.* New York: Macmillan.

[7] Talatizi C. et al., FED 159, 111867, 2020

[8] Siegel, R. and Howell, J.R. Thermal Radiation heat transfer, 4th edition, CRC Press 2001

[9] Dutre P., Bekaert P., Bala K., Advanced Global Illumination, 2nd Ed., A. K. Peters Ltd, 2006

[10] Sillion F., Puech C., Radiosity and Global Illumination, M. Kaufman Publishers Inc., 1994

[11] Sara C. Francisco et al., 2014, Calculation of view factors for complex geometries using Stokes' theorem, Journal of Building Performance Simulation.

[12] Le Bohec M. et al., Congrès Français de Thermique 2019, doi: 10.25855/SFT2019-078

[13] Le Bohec M. et al., Congrès Français de Thermique 2020, doi: 10.25855/SFT2020-073

[14] Michael F. Modest, Radiative Heat Transfer, 3rd Edition, Academic Press 2013

[15] Leduc G. et al., International Journal of Heat and Mass Transfer, Elsevier, 2004, 47 (14-16), pp.3291-3300. doi: 10.1016/j.ijheatmasstranfer.2004.03.005

[16] Richard C. Aster, Brian Borchers, Clifford H. Thurber, Parameter Estimation and Inverse Problems, Academic Press, 2013.

[17] B. Rémy, S. André, Thermal Measurements and Inverse Techniques, Chapter 9 Nonlinear Estimation Problems, CRC Press 2011

[18] James V. Beck and Kenneth J. Arnold, Parameter Estimation in Engineering and Science, John Wiley and Sons, 1977

[19] D. Immel et al., A Radiosity Method for Non-Diffuse Environments, Proceedings of the 13st Annual Conference on Computer Graphics and Interactive Techniques, SIGGRAPH, 1986.

[20] A.N. Tikhonov, V.Y. Arsenin, Solutions of Ill-Posed Problems, V.H. Winston&Sons, Washington, D.C., 1977.